Surface Science 606 (2012) 1670–1679

Contents lists available at SciVerse ScienceDirect

Surface Science

journal homepage: www.elsevier.com/locate/susc

Atomic and molecular adsorption on Pd(111)

Jeffrey A. Herron, Scott Tonelli, Manos Mavrikakis *

Department of Chemical and Biological Engineering, University of Wisconsin – Madison, Madison, WI 53706, USA

ARTICLE INFO

Article history:
Received 2 June 2012
Accepted 5 July 2012
Available online 16 July 2012

Keywords:
Density functional theory
Palladium
Catalysis
Adsorption
Binding energies
Vibrational frequencies
Diffusion

ABSTRACT

The adsorption properties of a variety of atomic species (H, O, N, S, and C), molecular species (N_2, HCN, CO, NO, and NH_3) and molecular fragments (CN, NH_2, NH, CH_3, CH_2, CH, HNO, NOH, and OH) are calculated on the (111) facet of palladium using periodic self-consistent density functional theory (DFT–GGA) calculations at ¼ ML coverage. For each species, we determine the optimal binding geometry and corresponding binding energy. The vibrational frequencies of these adsorbed species are calculated and are found to be in good agreement with experimental values that have been reported in literature. From the binding energies, we calculate potential energy surfaces for the decomposition of NO, CO, N_2, NH_3, and CH_4 on Pd(111), showing that only the decomposition of NO is thermochemically preferred to its molecular desorption.

1. Introduction

Palladium is an important catalyst that is used in a number of industrial reactions including selective hydrogenation of unsaturated hydrocarbons [1–7], water–gas shift reaction, and as part of the three-way catalyst used in treating automobile exhaust gases [8–15]. Palladium and palladium-based alloys have also been shown to be highly active catalysts for the electrocatalytic reduction of oxygen, one of the most challenging reactions in polymer electrolyte membrane (PEM) fuel cells [16]. Palladium catalysts are used for formic acid electro-oxidation [17,18]. Palladium is also an efficient catalyst in cross-coupling reactions including the Suzuki [19] and Heck [20] reactions. Further, because of its high hydrogen permeability, Pd has been used as the basis of highly selective separation membranes and membrane reactors [21–23].

Hydrogen adsorption on Pd is a widely studied subject because of the facile hydrogen permeation into the subsurface and bulk of Pd. Temperature programmed desorption (TPD) studies indicate formation of chemisorbed, solid solution (α-phase), and hydride phases (β-phase) on Pd(111) [24,25]. Studies of palladium catalyzed hydrogenation reactions suggest the importance of subsurface hydrogen [5–7,26]. Previous studies of subsurface hydrogen in Ni(111) have demonstrated experimentally [27], and theoretically [28], the unique ability of subsurface hydrogen to hydrogenate species upon emerging to the surface. On palladium, hydrogen has been studied using a number of experimental techniques including TPD [29], low-energy electron diffraction (LEED) [24,29,30], scanning tunneling microscopy (STM) [31–34], angle-resolved photoelectron spectroscopy (ARPES) [35], high resolution electron energy loss spectroscopy (HREELS) [36] and incoherent inelastic neutron scattering (IINS) [37].

Oxygen is an important intermediate for a number of reactions using Pd catalysts including methane oxidation [38–42], CO oxidation and NO reduction [10,11,15] as part of the three-way catalyst, and oxygen reduction reaction (ORR) [43]. A number of experimental techniques have been utilized to study oxygen on Pd including: TPD [44], LEED [44–47], ellipsometry [46], Auger electron spectroscopy (AES) [46], X-ray photoelectron spectroscopy (XPS) [46], STM [44,48–50], HREELS [51], and electron energy loss spectroscopy (EELS) [52].

Sulfur poisoning is a major problem in Pd-catalyzed hydrocarbon processing [1] and also causes deactivation of Pd-based hydrogen separation membranes [53]. Experimentally, sulfur on Pd has been studied by LEED [54], scanning tunneling spectroscopy (STS) [55], STM [55–57], AES [56], surface extended X-ray absorption fine structure (SEXAFS) [58], and normal incidence X-ray standing wave (NIXSW) [58].

NO has been studied extensively on Pd surfaces as this interaction is most relevant to car exhaust cleanup [10,11,15]. Experimental studies of NO interactions with Pd have been done using LEED [59,60], temperature desorption spectroscopy (TDS) [59], TPD [61], and HREELS [61,62].

CO adsorption on Pd is of fundamental importance to understanding its oxidation on the three-way catalyst [10,11,15], poisoning of fuel cell electrodes [17,63], and permeation of hydrogen through separation membranes [64]. For those reasons, CO has been studied by modulated beam experiments [65], (TDS) [66,68], single-crystal microcalorimetry [67], sum frequency generation spectroscopy (SFG) [68,69], LEED [68], AES [68], infrared reflection–absorption spectroscopy (RAIRS) [70], and STM [71–73].

* Corresponding author.
E-mail address: manos@engr.wisc.edu (M. Mavrikakis).

0039-6028/$ – see front matter © 2012 Elsevier B.V. All rights reserved.
doi:10.1016/j.susc.2012.07.003

Hydroxyl species (OH) are essential intermediates involved in the interactions of water [74–79] with metal surfaces in heterogeneous catalysis and in electrochemical oxygen reduction reaction [43]. Zhu et al. studied OH adsorption on Pd(111) using HREELS [80], while Andrae et al. calculated the desorption energy on polycrystalline Pd using microcalorimetry [76].

Here we present a database of adsorption energies, adsorption geometries, vibrational frequencies, and diffusion barriers all calculated with DFT–GGA, for common, small and industrially relevant adsorbates on the thermodynamically most stable facet of palladium, Pd(111). These adsorbates include atomic species (H, O, N, S, C), molecular species (N_2, NH_3, CO, NO, and HCN), and molecular fragments (CN, NH_2, NH, CH_3, CH_2, CH, HNO, NOH, and OH). The present paper represents a follow-up of other database papers we have published for similar atomic and molecular adsorption properties of these species on Rh(111) [81], Ir(111) [82], and Pt(111) [83]. The computational setup and methods used in all these papers are practically identical, thereby allowing for a comparison of adsorption properties of various species across several catalytic transition metal single crystal surfaces. Our data can be added to other electronically accessible databases, which have started appearing recently [84].

2. Methods

All calculations are performed using DACAPO [85,86]. A 2×2 unit cell is used to construct a four layer Pd(111) slab. This corresponds to a surface coverage of 1/4 ML when there is only one adsorbate per unit cell. The unit cell is repeated in a super cell geometry with successive slabs separated by a vacuum region equivalent to five metal layers. Adsorption is allowed on only one of the two exposed surfaces, with the electrostatic potential adjusted accordingly [87,88]. The top two layers of the slab are allowed to relax. The surface Brillouin zone is sampled at 18 special Chadi–Cohen k-points [89].

The Kohn–Sham one-electron valence states are expanded in a basis of plane waves with kinetic energies up to 25 Ry, whereas the ionic cores are described by ultrasoft Vanderbilt pseudopotentials [90]. In order to be consistent with our previous similar studies [81–83], the exchange–correlation potential and energy are described self-consistently using the GGA-PW91 functional [91,92]. The electron density is determined by iterative diagonalization of the Kohn–Sham Hamiltonian, Fermi-population of the Kohn–Sham states ($k_BT=0.1$ eV), and Pulay mixing of the resulting electronic density [93]. Total energies are then extrapolated to $k_BT=0$ eV.

The calculated gas-phase atomization energies for some of the adsorbate species are shown in Table 1, along with available experimental values [94] at 0 K. In addition to the PW91 results, we also list values calculated non-self-consistently using the RPBE functional [85]. As can be seen, the functionals did not consistently exhibit over-binding or under-binding with respect to the experimental values. The calculated PW91 equilibrium lattice constant for bulk Pd is 3.99 Å, in close agreement with the experimentally determined value of 3.89 Å [95].

Binding energies calculated using both exchange–correlation functionals will be presented below, with the RPBE values always enclosed in square brackets. The binding energies (E_b) are calculated with respect to a clean relaxed Pd(111) slab ($E_{substrate}$) and the respective free adsorbate in the gas phase ($E_{gas\text{-}phase\ adsorbate}$), i.e., $E_b = E_{total} - E_{substrate} - E_{gas-phase\ adsorbate}$.

Convergence of binding energies with respect to various calculation parameters is verified. The deformation energy (ΔE), i.e., the change in surface energy due to the adsorption of an adsorbate, is calculated by subtracting the energy of the relaxed, clean surface (E_{clean}), from the energy of the relaxed surface, frozen after the adsorption of the adsorbate ($E_{relaxed,\ adsorbate\ removed}$), but with the adsorbate removed. ($\Delta E = E_{relaxed,\ adsorbate\ removed} - E_{clean}$; note, this is a positive quantity). The harmonic vibrational frequencies of an adsorbate are determined from the diagonalization of the mass-weighted Hessian matrix. The second derivatives of energy are calculated using a finite difference approximation [96]. A vibrational mode is considered dipole-active if a non-zero intensity is calculated from the gradient of the dipole moment (calculated using a finite difference approximation) [97]. The diffusion barrier of an adsorbate is estimated by first identifying a plausible diffusion path, which connects neighboring minima on the potential energy surface (PES) via a metastable site, and then calculating the energy difference between the lowest minimum and the metastable state on that path. In some cases, the geometry of the adsorbate is fixed with respect to its x and y coordinates, allowing only the z-coordinate (and the slab) to relax. These cases are indicated explicitly in Table 4.

3. Results and discussion

Here, we describe the results of our calculations, including the binding energies and site preferences for the adsorbates (Table 2 and Table 7), their adsorption geometries (Table 5 and Fig. 2), the deformation to the surface due to adsorption (Table 6), and estimates for diffusion barriers (Table 4). We also report dipole-active vibrational frequencies for the adsorbed species (Table 3, Table 8, and Table 9).

3.1. Atomic species

3.1.1. Hydrogen

Hydrogen binds on fcc, hcp, and top sites, while the bridge site is unstable. For the fcc, hcp, and top sites, the calculated PW91 [RPBE in

Table 1
Calculated and experimental gas-phase atomization energies at 0 K.

Species	Atomization energy (eV)		
	PW91	RPBE	Exp.
N_2	9.63	9.47	9.76
NO	6.73	6.50	6.51
NH_3	12.74	12.50	12.00
NH_2	7.96	7.50	7.36
NH	3.74	3.38	3.40
CO	10.96	10.59	11.11
CH_4	18.08	17.74	17.02
CH_3	13.39	13.16	12.54
CH_2	8.49	8.37	7.81
CH	3.65	3.64	3.45
OH	4.60	4.53	4.41

The species here are those for which experimental values are available. The experimental values are taken from reference [94].

Table 2
Binding energies in PW91 [RPBE in brackets] and site preferences of atomic species on Pd(111); the binding energy for the most stable site for each species is shown in bold.

Adsorbate	Preferred site		Binding energy (eV)			
	Calc.	Exp.	Top	fcc	hcp	Exp.
H	fcc	fcc[a]	−2.29 [−2.14]	**−2.88 [−2.69]**	−2.84 [−2.66]	[b]
O	fcc	fcc[c]		**−3.79 [−3.20]**	−3.61 [−3.03]	[d]
N	fcc			**−4.01 [−3.55]**	−3.91 [−3.44]	
S	fcc	fcc[e]		**−4.66 [−4.12]**	−4.59 [−4.06]	
C	hcp			−6.27 [−5.78]	**−6.30 [−5.80]**	

RPBE values are enclosed in square brackets. The zero reference energy corresponds to the gas-phase atom at infinite separation from the palladium slab. The bridge site was found to be unstable for all atomic species. For H, in particular, binding energies were also calculated for sites between the first and second layers: the octahedral (−2.54 [−2.36]eV), tetrahedral under top-site (−2.49 [−2.32]eV), and tetrahedral under hcp-site (−2.53 [−2.34]eV).

[a] LEED [24,29], STM [31].

[b] Experimental heats of adsorption for hydrogen are available from TPD [29] and molecular beam studies [98], see main text for details.

[c] LEED [47].

[d] Experimental heats of adsorption of oxygen are available from thermal desorption [45] and TPD [44], see main text for details.

[e] NIXSW [58], LEED [54], STM [55].

Table 3
Vibrational frequencies for metal-adsorbate stretch of adsorbed atomic species on Pd(111) in their most stable site.

Adsorbate	Calculated (cm^{-1})	Experimental (cm^{-1})
H (fcc)	964	1000[a], 968[b]
O (fcc)	442	472[c], 480[d]
N (fcc)	508	
S (fcc)	324	
C (hcp)	535	

Experimental values are provided when available; values are presented in their original units in the main body of this paper.
[a] HREELS [36].
[b] IINS [37].
[c] HREELS [51].
[d] HREELS [52].

brackets] binding energies are are −2.88 [−2.69], −2.84 [−2.66], and −2.29 [−2.14] eV, respectively. Our results are in good agreement with previous DFT studies [99–105]. For more direct comparisons with experimental data, we also calculate the heat of adsorption for a single H atom versus gas-phase hydrogen (1/2 H_2): −0.59 eV, −0.56 eV, and 0.00 eV, for the fcc, hcp, and top sites, respectively. Since hydrogen permeation is an important property of Pd, we calculate the binding energy for sites between the top Pd atomic layer and the layer right below that, finding −2.54 [−2.36] eV for the octahedral site, −2.53 [−2.34] eV for the tetrahedral site beneath the hcp site, and −2.49 [−2.32] eV for the tetrahedral site beneath the top site. TPD [29] studies determined a heat of adsorption of −20.8 kcal/mol of H_2 (−0.45 eV per H atom), whereas molecular beam studies [98] have found that the heat of adsorption per H atom varies from −0.46 eV at low coverage to −0.40 eV at saturation. Both studies agree well with our results. LEED [24,29] and STM [31,32] studies have found a number of different adsorption structures, including $(\sqrt{3}\times\sqrt{3})$R30°-H (0.33 ML coverage), $(\sqrt{3}\times\sqrt{3})$R30°-2H (0.66 ML coverage), and a 1×1 structure (greater than 0.66 ML coverage). In particular, it has been concluded that in the $(\sqrt{3}\times\sqrt{3})$R30° phases, H atoms occupy fcc hollow sites. Felter et al. found that the H atom resides 0.80 to 0.85 Å above the first Pd layer [24] (Pd–H bond length of 1.78 to 1.80 Å), while an earlier study using both ARPES and theoretical calculations found H in threefold-hollow sites with a Pd–H bond distance of 1.69 Å [35]. We find that H resides 0.78 Å above the first Pd layer, with a corresponding Pd–H bond length of 1.82 Å (see Fig. 2), in good agreement with the experimental data. Our vibrational frequency calculations for fcc-bound H provide a surface parallel stretch at 861 cm^{-1} and a perpendicular stretch at 964 cm^{-1}. HREELS studies found losses corresponding to a parallel stretch at 0.096 eV (774 cm^{-1}) and a perpendicular stretch at 0.124 eV (1000 cm^{-1}) for hollow-site bound H [36], while IINS measurements on Pd deposited on carbon black showed vibrations at 0.094 eV (758 cm^{-1}), 0.101 eV (815 cm^{-1}), and 0.120 eV (968 cm^{-1}) [37]. LEED studies showed rapid surface diffusion above 55 K [30], while STM studies have estimated a surface diffusion barrier of 0.09 eV at 37 K [31]. We estimate a diffusion barrier from the fcc to the hcp site of 0.15 [0.14] eV. Adsorption slightly deforms the Pd surface, with a calculated deformation energy of 0.01 [0.00] eV.

Table 4
Estimated surface diffusion barriers of adsorbed species on Pd(111).

Adsorbate	Diffusion barrier (eV)		Diffusion path	Exp. (eV)
	PW91	RPBE		
H[a]	0.15	0.14	fcc-br-hcp	0.09[c]
O[b]	0.60	0.54	fcc-br-hcp	0.40–0.50[d]
N[a]	0.77	0.74	fcc-br-hcp	
S[a]	0.41	0.39	fcc-br-hcp	
C[b]	0.80	0.78	hcp-br-fcc	
N_2	0.16	0.24	Top-br	
NH_3[b]	0.41	0.32	Top-br-top	
NH_2	0.52	0.40	br-top	
NH[b]	0.74	0.68	fcc-br-hcp	
CN[a]	0.20	0.17	fcc-br-hcp	
NO[a]	0.36	0.32	fcc-br-hcp	
HNO	0.51	0.31	br-top	
NOH[b]	0.79	0.73	fcc-br-hcp	
CO	0.19	0.17	hcp-br-fcc	0.118[e]
CH_3[a]	0.23	0.32	Top-br-top	
CH_2	1.09	1.03	br-top	
CH[b]	0.75	0.76	fcc-br-hcp	
OH	0.06	0.11	br-fcc	

[a] Fixing x and y coordinates of the atom through which the adsorbate binds (e.g. for CN only the x and y coordinates of C were fixed).
[b] Fixing: x and y coordinates of the atom through which the adsorbate binds (e.g. for NH_3 only the x and y coordinates of N were fixed) and all coordinates of slab atoms.
[c] STM [31].
[d] STM [48,50].
[e] STM [73].

Table 5
Adsorption geometry on Pd(111): listed parameters are defined in Fig. 1.

Adsorbate	Z_{A-Pd} (Å)	ΔZ (Å)	d_{Pd-Pd} (Å)[a]	d_{A-B} (Å)
H (fcc)	0.784	0.027	2.847	
O (fcc)	1.182	0.042	2.894	
N (fcc)	1.051	0.073	2.856	
S (fcc)	1.559	0.040	2.892	
C (hcp)	0.982	0.066	2.863	
N_2 (top)	2.067	0.123	2.822	1.128
NH_3 (top)	2.213	0.068	2.822	1.023
NH_2 (br)	1.553	0.090	2.839	1.024
NH (fcc)	1.120	0.061	2.906	1.029
HCN (top–top)	1.631	0.057	2.840	1.099 (H–C), 1.232 (C–N)
CN (fcc)	1.369	0.030	2.852	1.201
NO (fcc)	1.258	0.077	2.857	1.208
HNO (br-tilted)	1.535	0.061	2.858	1.037 (N–H), 1.313 (N–O)
NOH (fcc-bent)	1.139	0.071	2.900	1.388 (N–O), 0.989 (O–H)
CO (hcp)	1.311	0.061	2.829	1.193
CH_3 (top)	2.068	0.153	2.825	1.097
CH_2 (br)	1.475	0.097	2.798	1.101
CH (fcc)	1.112	0.075	2.850	1.102
OH (br)	1.633	0.060	2.847	0.986

[a] The equilibrium Pd–Pd bond distance is 2.818 Å

3.1.2. Oxygen

Atomic oxygen binds to fcc and hcp sites, with binding energies of −3.79 [−3.20] eV and −3.61 [−3.03] eV, respectively, with respect to gas phase atomic oxygen. With the calculated gas phase

Table 6
Calculated deformation energy (ΔE) upon adsorption of each species on Pd(111). Only information on the respective preferred site for each adsorbate is listed.

Adsorbate	Site	ΔE (eV)	
		PW91	RPBE
H	fcc	0.01	0.00
O	fcc	0.07	0.06
N	fcc	0.05	0.02
S	fcc	0.05	0.03
C	hcp	0.05	0.02
N_2	Top	0.03	0.03
NH_3	Top	0.01	0.01
NH_2	br	0.08	0.07
NH	fcc	0.08	0.06
HCN	Top–top	0.04	0.02
CN	fcc	0.01	0.00
NO	fcc	0.05	0.02
HNO	br-tilted	0.09	0.08
NOH	fcc-bent	0.09	0.07
CO	hcp	0.02	0.00
CH_3	Top	0.04	0.03
CH_2	br	0.04	0.02
CH	fcc	0.03	0.00
OH	br	0.06	0.06

Table 7
Binding energies in PW91 [RPBE in brackets] for stable sites and site preferences of molecular species and molecular fragments on Pd(111); the binding energy for the most stable site for each species is shown in bold.

Adsorbate	Preferred site		Binding energy (eV)				
	Calc.	Exp.	Top	fcc	hcp	Bridge	Exp.
N_2	Top		**−0.23 [0.08]**	−0.02 [0.39]		−0.07 [0.32]	
NH_3	Top		**−0.62 [−0.27]**				−0.75[a]
NH_2	Bridge		−1.63 [−1.20]			**−2.15 [−1.59]**	
NH	fcc			**−3.45 [−2.82]**	−3.30 [−2.68]		
HCN	Bridge		−0.90 [−0.42]			**−0.91 [−0.38]**	−0.39[b]
CN	fcc	See text[c]	−3.08 [−2.77]	**−3.68 [−3.25]**	−3.63 [−3.20]		
NO	fcc	Bridge[d]	−1.37 [−0.95]	**−2.07 [−1.49]**	−2.04 [−1.46]		−1.34,[e] −1.65[f]
HNO	Bridge		−3.45 [−2.91]			**−3.97 [−3.22]**	
NOH	fcc			**−3.90 [−3.16]**	−3.78 [−3.04]		
CO	hcp	fcc[g]	**−1.29 [−0–.97]**	−1.95 [−1.54]	**−1.96 [−1.55]**	−1.77 [−1.39]	−1.39,[h] −1.54[i]
CH_3	Top		**−1.67 [−1.32]**				
CH_2	Bridge					**−3.56 [−3.05]**	
CH	fcc	Hollow[j]		**−5.91 [−5.31]**	−5.89 [−5.28]		
OH	Bridge		−1.93 [−1.48]	−2.15 [−1.55]	−2.02 [−1.45]	**−2.21 [−1.66]**	−2.34[k]

The zero energy reference corresponds to gas-phase species at infinite separation from the palladium slab. Experimental values are provided where available.
[a] TPD on Pd foil [117].
[b] TDS [118].
[c] NEXAFS [119] and XPS [120] suggest CN adsorbs parallel to the surface.
[d] HREELS [61,62].
[e] Thermal desorption [59].
[f] TPD [61].
[g] SFG Spectroscopy and LEED [68].
[h] Modulated beam [65].
[i] TDS [66]; Single-crystal microcalorimetry [67].
[j] SFG spectroscopy and XPS [121].
[k] Microcalorimetry and LIF on polycrystalline Pd [76].

O_2 bond energy at 5.64 eV (PW91), these numbers correspond to dissociative heats of adsorption for O_2 of −1.95 [−1.21] eV and −1.58 [−0.86] eV, respectively. Our findings are in reasonable agreement with previous DFT studies [47,104–108]. Further, at low temperature, Conrad et al. used LEED to find (2×2) and (√3×√3)R30° structures with an estimated adsorption energy of ~−55 kcal/mol (−2.38 eV) [45]. Above 1000 K, they detected more strongly bound oxygen, which they assigned to formation of a PdO phase. Voogt et al. studied oxygen adsorption on Pd(111) at temperatures above 470 K and pressure above 10^{-4} Pa using ellipsometry, LEED, AES, and XPS [46]. They found three adsorption stages, (1) dissociative adsorption to a saturation coverage of 0.25 ML, (2) diffusion of oxygen atoms into the subsurface (only into the first layer, not the bulk), with a total coverage of 0.50 ML, and (3) formation of a surface oxide phase. STM, LEED, and TPD studies suggested a similar mechanism of oxide formation, with an initial oxygen heat of adsorption of −50.2 kcal/mol (−2.18 eV) [44]. This and the previous heat of adsorption are in reasonable agreement with our calculated values. It has been suggested that these oxide phases may be important in a number of applications including lean oxidation of methane [38–40]. HREELS studies at 300 K and EELS studies at 200 K found characteristic Pd–O modes at 58.6 meV (472 cm^{-1}) [51] and 480 cm^{-1} [52], respectively, in agreement with our calculated value of 442 cm^{-1}. In the fcc site, atomic oxygen adsorbs 1.18 Å above the Pd surface layer, which is lifted 0.04 Å from its equilibrium position, in excellent agreement with LEED studies of the (2×2) phase [47]. We estimate the deformation energy induced by ¼ ML of O adsorption to be 0.07 [0.06] eV. Finally, STM studies have found a 0.4 to 0.5 eV diffusion barrier [48,50], in reasonable agreement with the 0.60 [0.54] eV barrier that we calculated here.

3.1.3. Nitrogen

Nitrogen atoms adsorb on fcc and hcp sites with binding energies of −4.01 [−3.55] eV and −3.91 [−3.44] eV, respectively. In fcc sites, N binds 1.05 Å above the first Pd layer, causing outward expansion of Pd by 0.07 Å. The associated deformation energy is calculated to be 0.05 [0.02] eV. The diffusion barrier from the fcc to hcp site is estimated to be 0.77 [0.74] eV. A Pd–N vibrational stretching mode is calculated at 508 cm^{-1}. The structural and adsorption energies that we calculate agree well with a previous DFT study [109]. Unfortunately, there is a lack of experimental data for atomic N adsorption on Pd(111), which would allow more detailed comparisons with our results.

3.1.4. Sulfur

Sulfur adsorbs strongly to fcc and hcp sites of Pd(111) with calculated binding energies of −4.66 [−4.12] eV and −4.59 [−4.06] eV, respectively. These binding energies are in good agreement with a previous DFT study [110]. In fcc sites, S binds 1.56 Å above the Pd surface, leading to a slight raising of the Pd surface by 0.04 Å and expansion of the Pd–Pd bond distance of adjacent Pd atoms by 0.07 Å. The associated deformation energy is found to be 0.05 [0.03] eV. LEED [54] analysis has revealed a room-temperature (√3×√3)R30° phase which transforms into a (√7×√7)R19.1° phase at approximately 450 K under exposure to H_2S. In the low-temperature phase, S atoms occupy fcc-hollow sites, in agreement with our results. STS and STM studies of the (√7×√7)R19.1° phase showed occupation of both fcc and hcp hollow sites [55]. Other studies have shown that the (√3×√3)R30° phase coexists with (2×2) stripes and triangles [111,112]. STM and AES have identified sulfur impurities in substitutional sites below the surface layer [56]. SEXAFS [58] studies of the (√3×√3)R30° phase provided a S–Pd nearest-neighbor bond-distance of 2.28+/−0.04 Å, in excellent agreement with the 2.29 Å bond distance that we find. We calculate a Pd–S vibrational mode of 324 cm^{-1}, and our estimate for the diffusion barrier of S from the fcc to hcp site is 0.41 [0.39] eV.

3.1.5. Carbon

Carbon atoms adsorb on fcc and hcp sites, with binding energies of −6.27 [−5.78] eV and −6.30 [−5.80] eV, respectively. These values are in good agreement with previous DFT studies [105,113,114]. Experimental characterization of atomic carbon adsorbed is scarce, though it has been suggested to be an important subsurface impurity in Pd(111) [6,56,115,116] because of its ability to affect hydrocarbon hydrogenation [5,6]. Therefore, we also calculate the binding energy of carbon in the first subsurface layer, finding the octahedral site to be more stable than the surface sites, with a binding energy of −7.00 [−6.48] eV. This

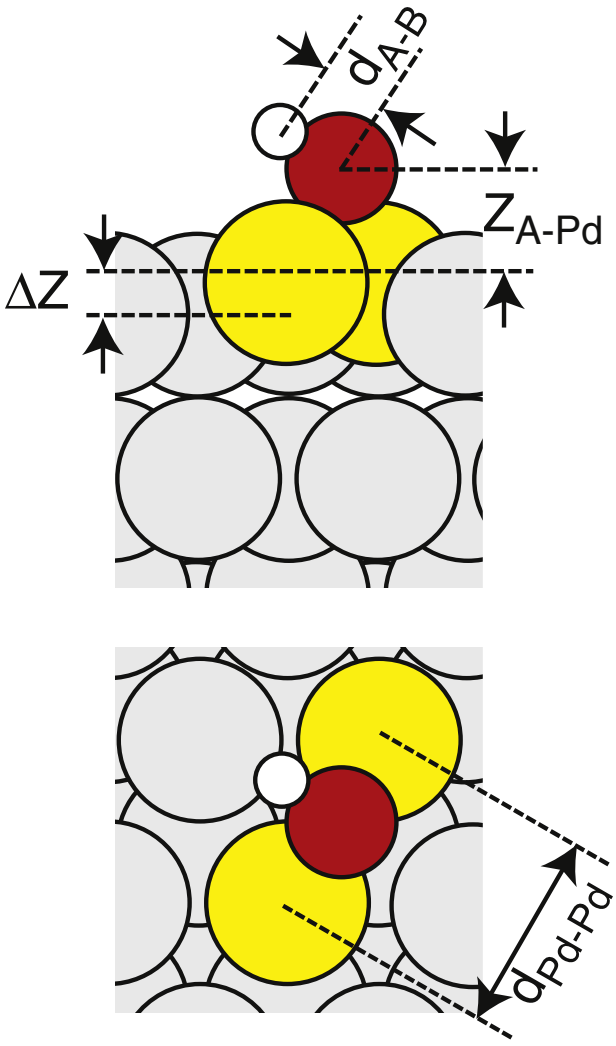

Fig. 1. Side (shown above) and top (shown below) views of species adsorbed on the Pd(111) slab. Definitions of the geometric parameters introduced in Table 5 for surface adsorbates are provided schematically. Z_{A-Pd} corresponds to the vertical distance between the adsorbate and the plane of the Pd atoms in contact with it. ΔZ_{Pd} is the change in the vertical distance between the plane of the palladium atoms in contact with the adsorbate and the plane of palladium atoms on a clean relaxed surface. d_{Pd-Pd} is the distance between two adjacent palladium atoms in contact with the adsorbate (or an average of these distances when bound in hollow sites). d_{A-B} is the bond length between atoms A and B within an adsorbed species. Pd atoms in contact with adsorbate are highlighted in yellow.

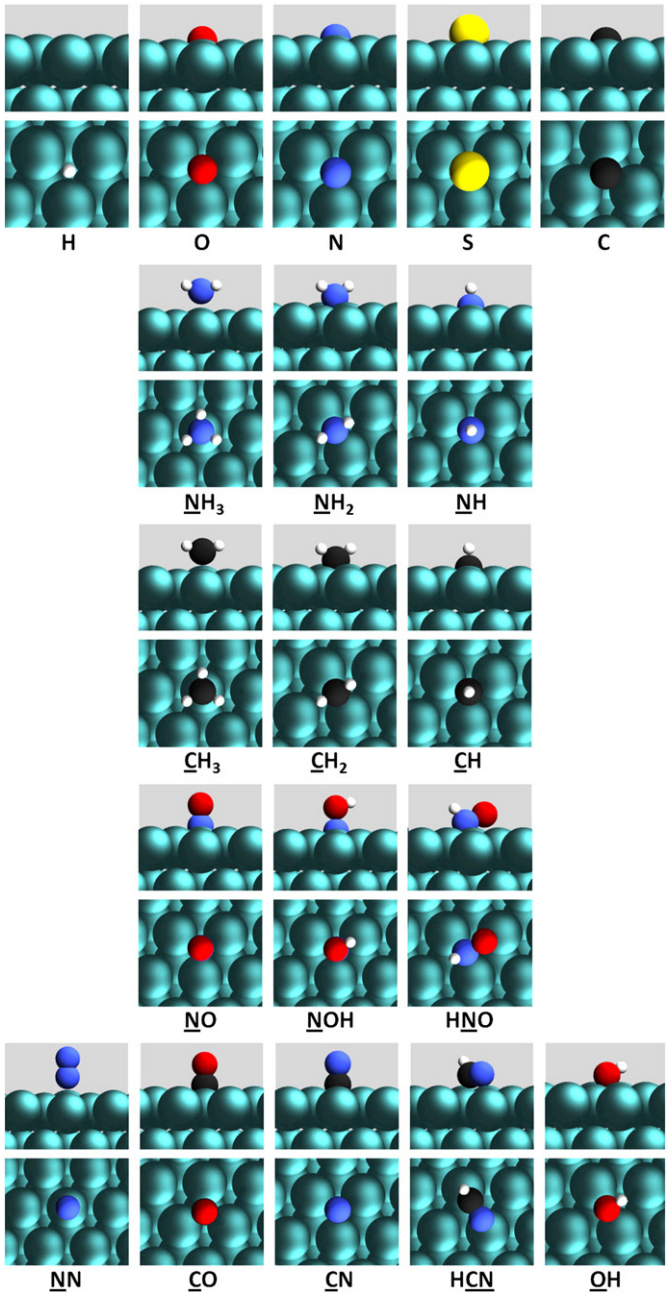

Fig. 2. Cross-section (above) and top view (below) of optimal adsorbate geometries on Pd(111). The atom(s) through which the adsorbate binds is(are) underlined in the adsorbate name given below each panel.

result is in agreement with STM studies that found subsurface carbon occupying octahedral sites [56] and a previous DFT study [116]. In hcp sites, C is bound 0.98 Å above the surface, with the Pd surface protruded 0.07 Å above its equilibrium position. The resulting deformation is estimated to cost 0.05 [0.02] eV. Diffusion from the hcp to fcc site through the bridge position is estimated to have a 0.80 [0.78] eV barrier. We calculate a Pd–C stretching mode of 535 cm^{-1}.

3.2. Adsorption of molecules and molecular fragments

3.2.1. Dinitrogen (N_2)

We calculate stable adsorption states for N_2 on the top, bridge, and fcc sites of Pd(111). The top state is the most stable, with a binding energy of −0.23 [0.08] eV, while the bridge and fcc states are significantly less stable with binding energies of −0.07 [0.32] eV and −0.02 [0.39] eV, respectively. In all sites, N_2 binds with the N–N bond perpendicular to the surface. On the top site, the N atom with which N_2 is bound to the surface is 2.07 Å above the Pd surface layer, with a 1.13 Å N–N bond length (see Fig. 2). The deformation energy of the adsorption is 0.03 [0.03] eV. An N–N vibrational mode is calculated at 2309 cm^{-1}, in good agreement with an HREELS loss at 290 meV (2340 cm^{-1}) [122]. We also calculate a dipole-active Pd–N_2 stretch at 261 cm^{-1}.

3.2.2. Ammonia (NH_3)

Ammonia adsorbs only at the top site of Pd(111) and with a modest binding energy (−0.62 [−0.27] eV), in reasonable agreement with the −17.4 kcal/mol (−0.75 eV) determined through TPD studies on a Pd foil [117]. Geometries and corresponding adsorption energies agree with a previous DFT study [109]. Ammonia is bound 2.21 Å above the Pd surface with N–H bond lengths of 1.02 Å (see Fig. 2). The deformation energy is 0.01 [0.01] eV. The calculated dipole-active vibrational frequencies are a symmetric

Table 8
Vibrational frequencies (cm^{-1}) of selected diatomic adsorbates on Pd(111).

Adsorbate	Pd–X		A–B	
	Calc.	Exp.	Calc.	Exp.
N_2 (top)	261		2309	2340[a]
NH (fcc)	494		3446	
CN (fcc)	330	300[b]	1974	1910[b]
NO (fcc)	294	331[c]	1637	1589[c], 1575[d]
NO (top)	479	484[c]	1793	1750[c], 1735[d]
CO (hcp)	325		1891	1850[e], 1823[f]
CH (fcc)	558		3025	
OH (bridge)	376	360[g]	3736	3400[g]

All modes listed are dipole-active. Experimental values are included where available. Pd–X refers to palladium–adsorbate (X) stretching mode, while A–B refers to the stretch of the intramolecular bond.
[a] HREELS [122].
[b] EELS [123].
[c] HREELS [62].
[d] HREELS [61].
[e] SFG spectroscopy [68].
[f] RAIRS [70].
[g] HREELS [80].

N–H bond stretch at 3431 cm^{-1}, a wagging mode at 959 cm^{-1}, and a Pd–NH_3 stretch at 269 cm^{-1}. We estimate a diffusion barrier of 0.41 [0.32] eV for ammonia diffusing across a bridge site.

3.2.3. NH_2, NH

NH_2 is stable on bridge and top sites with binding energies of −2.15 [−1.59] eV and −1.63 [−1.20] eV, respectively. On bridge sites, NH_2 is bound with the N atom 1.55 Å above the surface causing a 0.09 Å outward expansion of the Pd atoms. The associated deformation energy is 0.08 [0.07] eV. The N–H bond lengths are 1.02 Å. NH binds to fcc and hcp hollow sites with the N–H bond axis perpendicular to the surface. The binding energies are −3.45 [−2.82] eV and −3.30 [−2.68] eV, respectively. In fcc sites, N is 1.12 Å above the surface with a 1.03 Å N–H bond length. The adsorption expands the Pd–Pd bond distance of adjacent atoms by 0.08 Å, and the Pd atoms protrude 0.06 Å above their equilibrium position. The associated deformation energy is 0.08 [0.06] eV. These adsorption energies and geometries (see Fig. 2) agree with a previous DFT study [109]. For NH_2, two dipole active vibrational modes are calculated: a scissoring mode at 1435 cm^{-1} and a Pd–NH_2 stretch at 431 cm^{-1}. For NH we calculate two dipole active modes: the N–H bond stretch at 3446 cm^{-1} and the Pd–NH stretch at 494 cm^{-1}. The estimated diffusion barriers for NH_2 and NH are 0.52 [0.40] eV and 0.74 [0.68] eV, respectively.

3.2.4. HCN and CN

HCN adsorbs on Pd(111) in two isoenergetic configurations. These are a di-σ geometry in which the C and N atoms are both bound to top sites (see Fig. 2), and a second state where it is bound on a bridge site. The binding energies for these geometries are −0.90 [−0.42] eV and −0.91 [−0.38] eV, respectively. TDS measurements provided a heat of adsorption of −9.1 kcal/mol (−0.39 eV), significantly smaller than our calculated value [118]. In the di-σ geometry, we find a C–H bond length of 1.10 Å and a C–N bond length of 1.23 Å. In the bridge bound state, the C–H bond length is 1.10 Å, while the C–N bond is 1.25 Å. The deformation energy associated with the di-σ adsorption is 0.04 [0.02] eV. We find four dipole-active vibrational modes for the di-σ geometry. These are the C–H stretch at 3087 cm^{-1}, C–N stretch at 1723 cm^{-1}, a rocking mode at 442 cm^{-1}, and a C–H bond bending mode at 869 cm^{-1}. For the bridge bound geometry, we calculate a C–H stretching mode at 3052 cm^{-1}, C–N bond stretch at 1600 cm^{-1}, Pd–HCN stretch at 341 cm^{-1}, and a rocking mode at 436 cm^{-1}. HREELS studies of CN hydrogenation at room temperature gives energy losses at 1541 cm^{-1} and 3307 cm^{-1} [124,125], which are identified as C–N and C–H bond stretches, respectively. These frequencies are in reasonable agreement with those found for both calculated geometries.

CN binds most strongly to fcc sites, with a binding energy of −3.68 [−3.25] eV. It also binds to hcp sites with a binding energy of −3.63 [−3.20] eV, and top sites with a binding energy of −3.08 [−2.77] eV. In all cases, the species is bound through the carbon atom (1.37 Å above the surface for fcc site) with the C–N bond axis (C–N bond length calculated to be 1.20 Å for CN bound to an fcc site) perpendicular to the surface (see Fig. 2). In contrast, NEXAFS [119] and XPS [120] studies suggest that CN adsorbs parallel to the Pd(111) surface, which may be the result of different surface coverages between experiments and our calculations. However, EELS measurements of CN adsorption provided a C–N stretching mode of 1910 cm^{-1} and a Pd–CN mode of 300 cm^{-1} [123], which are in good agreement with the values calculated for our fcc-bound CN, 1974 cm^{-1} and 330 cm^{-1}, respectively. Adsorption

Table 9
Dipole-active vibrational frequencies (in cm^{-1}) of adsorbed polyatomic species in their optimal binding structures on Pd(111).

Modes	NH_3	NH_2	HCN		HNO	NOH	CH_3		CH_2	
	Calc.	Calc.	Calc.	Exp.	Calc.	Calc.	Calc.	Exp.	Calc.	Exp.
Symmetric IM stretch	3431		3087[a], 1723[b]	3307[d], 1541[e]	1136[f], 3302[g]	934[j], 3679[k]	2992	2932[o]	2955	2960[o], 2907[p]
Asymmetric IM stretch									3054	3043[o], 2984[p]
AS stretch	269	431				318	471		521	
Wagging	959						1084			
Scissoring		1435							1271	
Bending			869[c]		1284[h], 445[i]	1242[m]				
Rocking			442		278	422			558	

Experimental values are provided where available. IM stands for intramolecular, while AS stands for adsorbate-surface.
[a] ν(C–H).
[b] ν(C–N).
[c] C–H bending mode.
[d] ν(C–H), HREELS [124,125].
[e] ν(C–N), HREELS [124,125].
[f] ν(N–O).
[g] ν(N–H).
[h] N–H bending mode.
[i] N–O bending mode.
[j] ν(N–O).
[k] ν(O–H).
[m] O–H bending mode.
[o] RAIRS of CH_3I and CH_2I_2 [135].
[p] FTIR of CH_2Cl_2 On Pd/SiO_2 [136].

induces a slight, 0.03 Å protrusion of the surface Pd atoms, costing 0.01 [0.00] eV.

3.2.5. NO

NO is most stable on the fcc site with a binding energy of −2.07 [−1.49] eV, and slightly less stable on the hcp site, −2.04 [−1.46] eV. The top site is considerably less stable, with a binding energy of −1.37 [−0.95] eV, while the bridge site is unstable. Our results are in excellent agreement with previous DFT studies; yet, we note here that the bridge site has been found to be a stable adsorption site for a different overlayer structure at 0.33 ML (though 0.31 eV less stable than the fcc-bound) [126,127]. LEED studies revealed three prominent adsorption states: the low-coverage (i.e. 0.25 ML) γ-state, which has no long-range order, the α-state, p(2×2) at 0.50 ML NO coverage, and the β-state c(4×2) at 0.75 ML coverage [59,60]. STM [128] and another LEED [129] study have also shown the existence of a 0.625 ML c(8×2) structure. Thermal desorption measurements of the γ-state provided a binding energy of −31 kcal/mol (−1.34 eV) [59], while more recent TPD results have estimated a desorption activation energy of 38 kcal/mol (1.65 eV) [61]. HREELS studies between 20 and 300 K of the γ-state showed losses at 41 meV (331 cm^{-1}) and 197 meV (1589 cm^{-1}) which were attributed to bridge-bonded NO [62]. The α-state was characterized by two additional losses at 60 meV (484 cm^{-1}) and at 217 meV (1750 cm^{-1}). Another HREELS study found vibrational modes of 1575 cm^{-1} (bridge bound) and 1735 cm^{-1} (top bound) at 100 K and saturation coverage [61]. Our calculated modes for fcc-bound NO are 1637 cm^{-1} for the N–O bond stretch, and 294 cm^{-1} for Pd–NO stretch, in good agreement with the results for the γ–state. Because we were not able to find stable bridge-bound NO, we do not have modes for comparison for that state. We also calculate modes for top-site adsorption: the N–O stretch frequency is 1793 cm^{-1} and the Pd–NO stretch is 479 cm^{-1}, in good agreement with the experimental α-state modes. Vibrational frequencies from previous DFT studies are in agreement with our calculations, and it has been suggested that the experimental vibrational analysis using nitrosyl complexes as model systems for NO adsorption analysis may be incorrect [126]. On the fcc site, NO binds with the N atom 1.26 Å above the Pd surface, which is protruding by ~0.08 Å above its equilibrium position (see Fig. 2). The associated deformation energy is 0.05 [0.02] eV, and the N–O bond length adsorbed at the fcc site is calculated as 1.21 Å. We estimate a 0.36 [0.32] eV diffusion barrier for the fcc-bridge-hcp pathway.

3.2.6. NOH and HNO

NOH and HNO are possible intermediates in catalytic reduction of NO. In particular, NOH has been proposed as an intermediate when reacting NO with atomic hydrogen over Ru(0001) [130]. In their HREELS study, these authors attribute a peak at 983 cm^{-1} to the N–O stretch in NOH. NOH prefers to bind in fcc and hcp hollow sites of Pd(111), and the binding energies are −3.90 [−3.16] eV and −3.78 [−3.04] eV versus gas phase NO and atomic hydrogen, respectively. On the fcc site, NOH binds through the nitrogen atom with the N–O bond axis perpendicular to the surface and the O–H bond 16° with respect to the surface plane (see Fig. 2). The N atom is bound 1.14 Å above the surface, with 1.39 Å N–O and 0.99 Å O–H bond lengths. Adsorption induces a 0.07 Å protrusion of the Pd atoms, costing 0.09 [0.07] eV. In the fcc site, the N–O bond stretch in NOH is at 934 cm^{-1}, in reasonable agreement with the results on Ru(0001). We calculate other dipole active modes: O–H stretch at 3679 cm^{-1}, O–H bond bending at 1242 cm^{-1}, Pd–NOH stretch at 318 cm^{-1}, and a rocking mode at 422 cm^{-1}. We estimate a 0.79 [0.73] eV diffusion barrier from the fcc to hcp site.

HNO prefers to bind to the bridge site of Pd(111) through the N atom and also to the top site in a similar geometry. The binding energies with respect to gas phase NO and H are −3.97 [−3.22] eV and −3.45 [−2.91] eV, for the bridge and top site respectively, meaning that HNO and NOH are nearly isoenergetic species at their preferred sites (bridge and fcc) respectively on Pd(111). On the bridge site, the N–O bond axis is 18° with respect to the surface plane, and the N–H bond axis is 49° with respect to the surface plane (see Fig. 2). The corresponding N–O bond length is 1.31 Å and N–H bond length is 1.04 Å with the adjacent Pd atoms protruded by 0.06 Å. The associated deformation energy is 0.09 [0.08] eV. We find 5 dipole active vibrational modes: N–H stretch at 3302 cm^{-1}, N–H bond bending at 1284 cm^{-1}, N–O bond stretch at 1136 cm^{-1}, N–O bond bending at 445 cm^{-1}, and a rocking mode at 278 cm^{-1}. Diffusion from the bridge to top site is activated by 0.51 [0.31] eV.

3.2.7. CO

CO adsorbs on all high symmetry sites of Pd(111) with the hcp and fcc sites being the most stable. The binding energies are −1.96 [−1.55] eV (hcp), −1.95 [−1.54] eV (fcc), −1.77 [−1.39] eV (bridge), and −1.29 [−0.97] eV (top), in good agreement with previous DFT studies [71,105,131–133]. Modulated beam experiments have provided a heat of desorption of 32 kcal/mol (1.39 eV) [65], while a temperature desorption spectroscopy study estimated a zero-coverage desorption barrier of 35.5 kcal/mol (1.54 eV) at 200 K [66]. Single-crystal microcalorimetry experiments reported a heat of adsorption of −149 kJ/mol (−1.54 eV) [67]. The magnitudes of these experimental values are significantly smaller than our calculated results, but our calculated respective values for the RPBE functional (see Table 7) are much closer to those experimentally estimated. Morkel et al. studied CO adsorption using SFG, LEED, TDS, and AES finding a $(\sqrt{3}\times\sqrt{3})R30°$-1CO overlayer structure, corresponding to 0.33 ML coverage, where the CO occupy fcc sites [68], in agreement with STM studies [72]. Morkel et al. found a C–O vibrational mode at 1850 cm^{-1} [69], in reasonable agreement with: (i) a RAIRS study [70] at room temperature and low coverage which reported the mode at 1823 cm^{-1} and (ii) our calculated value of 1891 cm^{-1}. In hcp sites, CO is bound through the carbon atom with the C–O bond axis perpendicular to the surface. The carbon atom is 1.31 Å above the Pd surface, with a 1.19 Å C–O bond distance. The Pd surface layer is relaxed 0.06 Å outward, and the deformation energy is calculated as 0.02 [0.00] eV. The diffusion barrier was calculated as 0.118 eV using STM [73], in agreement with our calculated barrier of 0.19 [0.17] eV.

3.2.8. CH_3, CH_2, and CH

CH_x fragments are important intermediates in a number of industrial reactions including methanol decomposition [121,134], methane activation and methane oxidation [38–40]. CH_3, CH_2, and CH have been detected in a static secondary ion mass spectrometry (SSIMS) studies of methanol decomposition on Pd(111) [134]. Other studies of CH_x fragments have used SFG [121], XPS [121], while vibrational frequencies have been analyzed using methyl halides [135,136].

CH_3 prefers to adsorb on top sites with a binding energy of −1.67 [−1.32] eV, CH_2 on bridge sites with a binding energy of −3.56 [−3.05] eV, and CH on fcc and hcp sites with binding energies of −5.91 [−5.31] eV and −5.89 [−5.28] eV, respectively. On the top site, CH_3 is bound 2.07 Å above the surface, with C–H bond lengths of 1.10 Å. The Pd atom that binds CH_3 protrudes 0.15 Å from its equilibrium position, with an associated 0.04 [0.03] eV deformation energy. CH_2 is bound on bridge sites, 1.48 Å above the surface, with 1.10 Å C–H bond lengths. The interacting Pd atoms protrude 0.10 Å from equilibrium and the Pd–Pd bond distance decreases by 0.02 Å, with a deformation energy of 0.04 [0.02] eV. CH is bound in fcc sites 1.11 Å above the surface with 1.10 Å C–H bond lengths. The interacting Pd atoms protrude slightly by 0.07 Å, costing 0.03 [0.00] eV. These results are in good agreement with a previous DFT study [114], and the geometries are shown in Fig. 2. An SFG and XPS study of methanol decomposition on a CO saturated Pd(111) surface at 300 K showed a 2-fold decrease in the intensity of the hollow site bound CO, indicating that CH_x species, presumed to be CH, are poisoning hollow sites [121]. After removing the gas and annealing at 600 K, XPS shows desorption of CO, while the CH_x signature remains. For CH_3, we calculate three dipole active vibrational modes: a symmetric C–H bond stretch at

2992 cm^{-1}, a wagging mode at 1084 cm^{-1}, and a Pd–CH_3 stretch at 471 cm^{-1}. RAIRS studies of CH_3I on Pd(111) found a symmetric C–H stretch at 2932 cm^{-1}, in reasonable agreement with our results [135]. For CH_2, we find an asymmetric C–H stretch mode at 3054 cm^{-1} and a symmetric C–H stretch mode at 2955 cm^{-1}, in good agreement with a RAIRS study [135] of CH_2I_2 on Pd(111) finding modes at 3043 cm^{-1} and 2960 cm^{-1} and an FTIR study [136] of CH_2Cl_2 on Pd/SiO_2 finding modes at 2984 cm^{-1} and 2907 cm^{-1}. For fcc-bound CH, we calculate the C–H stretch at 3025 cm^{-1} and the Pd–CH stretch at 558 cm^{-1}. We estimate diffusion barriers for each species as 0.23 [0.32], 1.09 [1.03], and 0.75 [0.76] eV, for CH_3, CH_2, and CH, respectively.

3.2.9. OH

OH is able to bind to all four high symmetry sites studied. The binding energies for the bridge, fcc, hcp, and top sites are −2.21 [−1.66], −2.15 [−1.55], −2.02 [−1.45], and −1.93 [−1.48] eV, respectively. These values are in good agreement with previous DFT studies [104,137,138]. Using kinetic modeling, laser-induced fluorescence and microcalorimetry, Andrae et al. estimated the zero-coverage desorption energy of OH on polycrystalline Pd as 226 kJ/mol (2.34 eV), in reasonable agreement with our results [76]. On bridge sites, the O atom is bound 1.63 Å above the surface, with the O–H bond (0.99 Å) oriented 25° away from the surface (see Fig. 2). The interacting Pd atoms protrude 0.06 Å above their equilibrium position with a 0.06 [0.06] eV deformation energy. The estimated diffusion barrier from the bridge to fcc site is 0.06 [0.11] eV.

OH has been detected in a number of studies of water adsorption on Pd(111) [74,77–80]. Zhu et al. were able to characterize OH using HREELS by irradiating water bilayers at 100 K and then flashing to 170 K to remove remaining water molecules [80]. They found losses at 360 cm^{-1}, 900 cm^{-1} and 3400 cm^{-1}, which were assigned to Pd–OH stretching, O–H bending, and O–H stretching, respectively. For bridge bound OH (most stable state), we find corresponding modes at 376 cm^{-1}, 598 cm^{-1} and 3736 cm^{-1}, respectively.

3.3. Thermochemistry for NO, CO, N_2, NH_3, and CH_4 decomposition

Fig. 3 shows a potential energy surface for decomposition of NO, CO, N_2, NH_3, and CH_4 based on our calculated PW91 binding energies and gas-phase energetics.

Once NO adsorbs to the surface, it can either desorb or decompose. We investigate three routes for NO decomposition: (1) NO can be dissociated directly to N + O, (2) NO can be hydrogenated to HNO first and then dissociated to NH + O, or (3) NO can be hydrogenated to NOH first and then dissociated to N + OH. The reaction thermochemistry shows that the dissociation energy for HNO (−0.29 eV) and NOH (−0.18 eV) is slightly exothermic, while direct NO scission is endothermic by 1.00 eV. However, the energy to hydrogenate NO to HNO and NOH is 0.98 eV, and 1.04 eV, respectively. Therefore, based only on thermochemistry, none of these three routes is clearly favored. Though, when compared to desorption, the strong binding of NO favors decomposition.

Though CO adsorbs strongly (−1.96 eV) on Pd(111), CO dissociation is an endothermic process (2.89 eV), and as a result, desorption is favored over dissociation.

N_2 adsorbs very weakly (−0.23 eV) to Pd(111), while the N–N bond scission process is strongly endothermic (1.84 eV). Therefore, N_2 decomposition on Pd(111) is highly unfavorable.

The overall decomposition of NH_3 to N and H is mildly endothermic (ΔE = 0.11 eV) on Pd(111). All three dehydrogenation reaction steps ($NH_3^* + * \rightarrow NH_2^* + H^*$, $NH_2^* + * \rightarrow NH^* + H^*$, $NH^* + * \rightarrow N^* + H^*$) are endothermic up to ~0.3 eV. Though, due to the strong NH_3 binding (−0.63 eV) to Pd(111), it is only the third dehydrogenation step that raises the final state energy above that of gas-phase NH_3.

Methane decomposition is endothermic on Pd(111). Of the four dehydrogenation steps, the first two and the last are endothermic, while the third step ($CH_2^* + * \rightarrow CH^* + H^*$) is exothermic. The identified stability of the CH intermediate agrees with studies of methanol decomposition on Pd(111), showing that CH is stable past 600 K [121].

4. Conclusions

Using self-consistent, periodic density functional theory (DFT–GGA) calculations we find the adsorption properties of several atoms (H, O, N, S, and C), molecules (N_2, HCN, CO, NO, and NH_3) and molecular fragments (CN, NH_2, NH, CH_3, CH_2, CH, HNO, NOH, OH) on Pd(111). These properties include preferred binding sites and geometries, binding energies, estimates for diffusion barriers, and vibrational frequencies. Comparing these results to experimental and theoretical studies in the literature shows good agreement. Given the limited set of experimental values to compare with, we cannot conclude whether the PW91 or RPBE functional

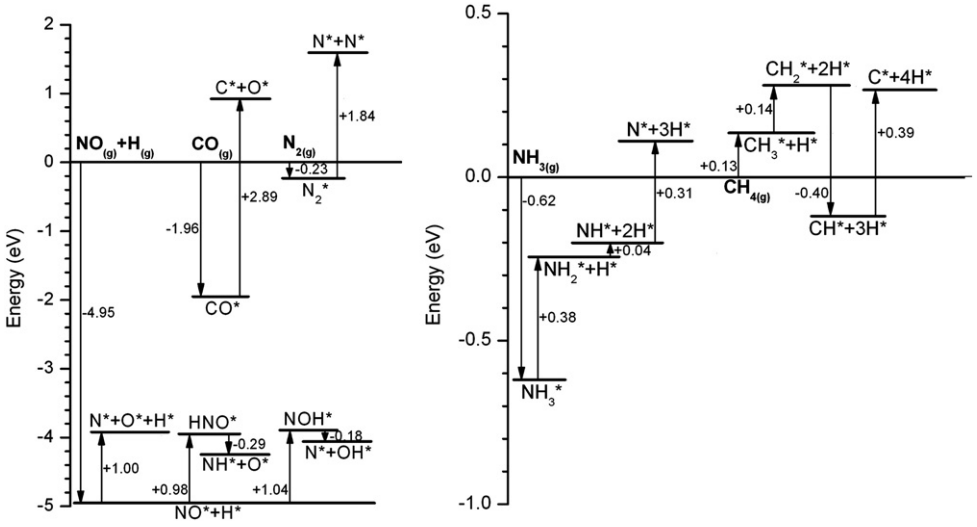

Fig. 3. Thermochemistry of molecular decomposition on Pd(111). The zero-energy reference state is the respective gas-phase molecule (also gas-phase H atom for NO + H) and a relaxed clean Pd(111) slab, at infinite separation. Energetics are calculated with the PW91 functional. The change in energy for each elementary step is shown next to the respective arrow. CH_4 and NH_3 decomposition are given on a separate graph; the energy scale is quite different than that for NO, CO, and N_2. Species marked with an * are adsorbed onto the Pd(111) surface.

provide binding energies which are more consistent with experiments. Finally, we use these results to develop simple potential energy surfaces for the decomposition of NO, CO, N_2, NH_3, and CH_4 on Pd(111). Of these five reactions, only the decomposition of NO is thermochemically favorable on Pd(111); for CO, N_2, NH_3, and CH_4, molecular desorption is preferred to their (complete) decomposition.

Acknowledgments

This paper is dedicated to Prof. Charlie T. Campbell's 10-year long outstanding service to the surface science community as editor-in-chief of this journal. We are grateful to him for that and wish him all the best for the future.

Work at UW-Madison was supported by the DOE-BES, Office of Chemical Sciences. JAH thanks the Air Products & Chemicals, Inc. for a graduate fellowship. Computational work was performed in part using supercomputing resources from the following institutions: EMSL, a National scientific user facility at Pacific Northwest National Laboratory (PNNL); the Center for Nanoscale Materials at Argonne National Laboratory (ANL); the National Center for Computational Sciences at Oak Ridge National Laboratory (ORNL); and the National Energy Research Scientific Computing Center (NERSC). EMSL is sponsored by the Department of Energy's Office of Biological and Environmental Research located at PNNL. CNM, NCCS, and ORNL are supported by the U.S. Department of Energy, Office of Science, under contracts DE-AC02-06CH11357, DEAC05-00OR22725, and DE-AC02-05CH11231, respectively.

References

[1] P. Albers, J. Pietsch, S.F. Parker, Journal of Molecular Catalysis A—Chemical 173 (2001) 275.
[2] A.N.R. Bos, K.R. Westerterp, Chemical Engineering and Processing 32 (1993) 1.
[3] H.J. Freund, Topics in Catalysis 48 (2008) 137.
[4] L. Burkholder, D. Stacchiola, W.T. Tysoe, Surface Review and Letters 10 (2003) 909.
[5] M. Wilde, K. Fukutani, W. Ludwig, B. Brandt, J.H. Fischer, S. Schauermann, H.J. Freund, Angewandte Chemie-International Edition 47 (2008) 9289.
[6] D. Teschner, J. Borsodi, A. Wootsch, Z. Revay, M. Havecker, A. Knop-Gericke, S.D. Jackson, R. Schlogl, Science 320 (2008) 86.
[7] D. Teschner, Z. Revay, J. Borsodi, M. Havecker, A. Knop-Gericke, R. Schlogl, D. Milroy, S.D. Jackson, D. Torres, P. Sautet, Angewandte Chemie-International Edition 47 (2008) 9274.
[8] K. Thirunavukkarasu, K. Thirumoorthy, J. Libuda, C.S. Gopinath, Journal of Physical Chemistry B 109 (2005) 13272.
[9] K. Thirunavukkarasu, K. Thirumoorthy, J. Libuda, C.S. Gopinath, Journal of Physical Chemistry B 109 (2005) 13283.
[10] D.R. Rainer, S.M. Vesecky, M. Koranne, W.S. Oh, D.W. Goodman, Journal of Catalysis 167 (1997) 234.
[11] M. Valden, J. Aaltonen, E. Kuusisto, M. Pessa, C.J. Barnes, Surface Science 307 (1994) 193.
[12] L.M. Carballo, T. Hahn, H.G. Lintz, Applied Surface Science 40 (1989) 53.
[13] D. Ciuparu, M.R. Lyubovsky, E. Altman, L.D. Pfefferle, A. Datye, Catalysis Reviews-Science and Engineering 44 (2002) 593.
[14] R.J. Farrauto, R.M. Heck, Catalysis Today 51 (1999) 351.
[15] V.I. Parvulescu, P. Grange, B. Delmon, Catalysis Today 46 (1998) 233.
[16] B. Lim, M.J. Jiang, P.H.C. Camargo, E.C. Cho, J. Tao, X.M. Lu, Y.M. Zhu, Y.N. Xia, Science 324 (2009) 1302.
[17] S. Ha, R. Larsen, R.I. Masel, Journal of Power Sources 144 (2005) 28.
[18] G.Q. Lu, A. Crown, A. Wieckowski, Journal of Physical Chemistry B 103 (1999) 9700.
[19] N. Miyaura, A. Suzuki, Chemical Reviews 95 (1995) 2457.
[20] I.P. Beletskaya, A.V. Cheprakov, Chemical Reviews 100 (2000) 3009.
[21] J. Shu, B.P.A. Grandjean, A. Vanneste, S. Kaliaguine, Canadian Journal of Chemical Engineering 69 (1991) 1036.
[22] R. Dittmeyer, V. Hollein, K. Daub, Journal of Molecular Catalysis A—Chemical 173 (2001) 135.
[23] I.-H. Svenum, J.A. Herron, M. Mavrikakis, H.J. Venvik, Catalysis Today (2012).
[24] T.E. Felter, E.C. Sowa, M.A. Vanhove, Physical Review B 40 (1989) 891.
[25] G.E. Gdowski, T.E. Felter, R.H. Stulen, Surface Science 181 (1987) L147.
[26] M. Wilde, K. Fukutani, Physical Review B 78 (2008).
[27] A.D. Johnson, S.P. Daley, A.L. Utz, S.T. Ceyer, Science 257 (1992) 223.
[28] V. Ledentu, W. Dong, P. Sautet, Journal of the American Chemical Society 122 (2000) 1796.
[29] H. Conrad, G. Ertl, E.E. Latta, Surface Science 41 (1974) 435.
[30] T.E. Felter, R.H. Stulen, M.L. Koszykowski, G.E. Gdowski, B. Garrett, Journal of Vacuum Science & Technology A—Vacuum Surfaces and Films 7 (1989) 104.
[31] T. Mitsui, M.K. Rose, E. Fomin, D.F. Ogletree, M. Salmeron, Surface Science 540 (2003) 5.
[32] L.C. Fernandez-Torres, E.C.H. Sykes, S.U. Nanayakkara, P.S. Weiss, Journal of Physical Chemistry B 110 (2006) 7380.
[33] T. Mitsui, M.K. Rose, E. Fomin, D.F. Ogletree, M. Salmeron, Nature 422 (2003) 705.
[34] T. Mitsui, E. Fomin, D.F. Ogletree, M. Salmeron, A.U. Nilekar, M. Mavrikakis, Angewandte Chemie-International Edition 46 (2007) 5757.
[35] W. Eberhardt, S.G. Louie, E.W. Plummer, Physical Review B 28 (1983) 465.
[36] H. Conrad, M.E. Kordesch, R. Scala, W. Stenzel, Journal of Electron Spectroscopy and Related Phenomena 38 (1986) 289.
[37] J.M. Nicol, J.J. Rush, R.D. Kelley, Physical Review B 36 (1987) 9315.
[38] H.H. Kan, J.F. Weaver, Surface Science 603 (2009) 2671.
[39] J.N. Carstens, S.C. Su, A.T. Bell, Journal of Catalysis 176 (1998) 136.
[40] A.K. Datye, J. Bravo, T.R. Nelson, P. Atanasova, M. Lyubovsky, L. Pfefferle, Applied Catalysis A—General 198 (2000) 179.
[41] K. Fujimoto, F.H. Ribeiro, M. Avalos-Borja, E. Iglesia, Journal of Catalysis 179 (1998) 431.
[42] J. Au-Yeung, K.D. Chen, A.T. Bell, E. Iglesia, Journal of Catalysis 188 (1999) 132.
[43] J. Zhang, Y. Mo, M.B. Vukmirovic, R. Klie, K. Sasaki, R.R. Adzic, Journal of Physical Chemistry B 108 (2004) 10955.
[44] G. Zheng, E.I. Altman, Surface Science 462 (2000) 151.
[45] H. Conrad, G. Ertl, J. Kuppers, E.E. Latta, Surface Science 65 (1977) 245.
[46] E.H. Voogt, A.J.M. Mens, O.L.J. Gijzeman, J.W. Geus, Surface Science 373 (1997) 210.
[47] A.P. Seitsonen, Y.D. Kim, S. Schwegmann, H. Over, Surface Science 468 (2000) 176.
[48] T. Mitsui, M.K. Rose, E. Fomin, D.F. Ogletree, M. Salmeron, Surface Science 511 (2002) 259.
[49] M.K. Rose, A. Borg, J.C. Dunphy, T. Mitsui, D.F. Ogletree, M. Salmeron, Surface Science 547 (2003) 162.
[50] M.K. Rose, A. Borg, J.C. Dunphy, T. Mitsui, D.F. Ogletree, M. Salmeron, Surface Science 561 (2004) 69.
[51] F.P. Leisenberger, G. Koller, M. Sock, S. Surnev, M.G. Ramsey, F.P. Netzer, B. Klotzer, K. Hayek, Surface Science 445 (2000) 380.
[52] R. Imbihl, J.E. Demuth, Surface Science 173 (1986) 395.
[53] J.K. Lee, H.K. Rhee, Journal of Catalysis 177 (1998) 208.
[54] M.E. Grillo, C. Stampfl, W. Berndt, Surface Science 317 (1994) 84.
[55] S. Speller, T. Rauch, A. Postnikov, W. Heiland, Physical Review B 61 (2000) 7297.
[56] M.K. Rose, A. Borg, T. Mitsui, D.F. Ogletree, M. Salmeron, Journal of Chemical Physics 115 (2001) 10927.
[57] J.G. Forbes, A.J. Gellman, J.C. Dunphy, M. Salmeron, Surface Science 279 (1992) 68.
[58] V.R. Dhanak, A.G. Shard, B.C.C. Cowie, A. Santoni, Surface Science 410 (1998) 321.
[59] H. Conrad, G. Ertl, J. Kuppers, E.E. Latta, Surface Science 65 (1977) 235.
[60] P. Kostelnik, T. Sikola, P. Varga, M. Schmid, Journal of Physics-Condensed Matter 21 (2009).
[61] D.T. Wickham, B.A. Banse, B.E. Koel, Surface Science 243 (1991) 83.
[62] M. Bertolo, K. Jacobi, Surface Science 226 (1990) 207.
[63] C. Rice, S. Ha, R.I. Masel, A. Wieckowski, Journal of Power Sources 115 (2003) 229.
[64] H. Amandusson, L.G. Ekedahl, H. Dannetun, Journal of Membrane Science 193 (2001) 35.
[65] T. Engel, Journal of Chemical Physics 69 (1978) 373.
[66] X.C. Guo, J.T. Yates, Journal of Chemical Physics 90 (1989) 6761.
[67] J.H. Fischer-Wolfarth, J.A. Farmer, J.M. Flores-Camacho, A. Genest, I.V. Yudanov, N. Rosch, C.T. Campbell, S. Schauermann, H.J. Freund, Physical Review B 81 (2010).
[68] M. Morkel, G. Rupprechter, H.J. Freund, Journal of Chemical Physics 119 (2003) 10853.
[69] M. Morkel, H. Unterhalt, M. Salmeron, G. Rupprechter, H.J. Freund, Surface Science 532 (2003) 103.
[70] A.M. Bradshaw, F.M. Hoffmann, Surface Science 72 (1978) 513.
[71] P. Sautet, M.K. Rose, J.C. Dunphy, S. Behler, M. Salmeron, Surface Science 453 (2000) 25.
[72] M.K. Rose, T. Mitsui, J. Dunphy, A. Borg, D.F. Ogletree, M. Salmeron, P. Sautet, Surface Science 512 (2002) 48.
[73] T. Mitsui, M.K. Rose, E. Fomin, D.F. Ogletree, M. Salmeron, Physical Review Letters 94 (2005).
[74] P.A. Thiel, T.E. Madey, Surface Science Reports 7 (1987) 211.
[75] M.A. Henderson, Surface Science Reports 46 (2002) 5.
[76] J.C.G. Andrae, A. Johansson, P. Bjornbom, A. Rosen, Surface Science 563 (2004) 145.
[77] C. Clay, L. Cummings, A. Hodgson, Surface Science 601 (2007) 562.
[78] A. Hodgson, S. Haq, Surface Science Reports 64 (2009) 381.
[79] M.J. Gladys, A.A. El Zein, A. Mikkelsen, J.N. Andersen, G. Held, Surface Science 602 (2008) 3540.
[80] X.Y. Zhu, J.M. White, M. Wolf, E. Hasselbrink, G. Ertl, Journal of Physical Chemistry 95 (1991) 8393.
[81] M. Mavrikakis, J. Rempel, J. Greeley, L.B. Hansen, J.K. Nørskov, Journal of Chemical Physics 117 (2002) 6737.
[82] W.P. Krekelberg, J. Greeley, M. Mavrikakis, Journal of Physical Chemistry B 108 (2004) 987.
[83] D.C. Ford, Y. Xu, M. Mavrikakis, Surface Science 587 (2005) 159.
[84] J.S. Hummelshoj, F. Abild-Pedersen, F. Studt, T. Bligaard, J.K. Nørskov, Angewandte Chemie-International Edition 51 (2012) 272.
[85] B. Hammer, L.B. Hansen, J.K. Nørskov, Physical Review B 59 (1999) 7413.
[86] J. Greeley, J.K. Nørskov, M. Mavrikakis, Annual Review of Physical Chemistry 53 (2002) 319.
[87] J. Neugebauer, M. Scheffler, Physical Review B 46 (1992) 16067.
[88] L. Bengtsson, Physical Review B 59 (1999) 12301.

[89] D.J. Chadi, M.L. Cohen, Physical Review B 8 (1973) 5747.
[90] D. Vanderbilt, Physical Review B 41 (1990) 7892.
[91] J.P. Perdew, J.A. Chevary, S.H. Vosko, K.A. Jackson, M.R. Pederson, D.J. Singh, C. Fiolhais, Physical Review B 46 (1992) 6671.
[92] J.A. White, D.M. Bird, Physical Review B 50 (1994) 4954.
[93] G. Kresse, J. Furthmuller, Computational Materials Science 6 (1996) 15.
[94] R.D.I. Johnson (Ed.) NIST Computational Chemistry Comparison and Benchmark Database, NIST Standard Reference, Database Number 101, 2004.
[95] CRC Handbook of Chemistry and Physics, New York, CRC Press, 2011.
[96] J. Greeley, M. Mavrikakis, Surface Science 540 (2003) 215.
[97] D. Porezag, M.R. Pederson, Physical Review B 54 (1996) 7830.
[98] T. Engel, H. Kuipers, Surface Science 90 (1979) 162.
[99] V. Pallassana, M. Neurock, L.B. Hansen, B. Hammer, J.K. Nørskov, Physical Review B 60 (1999) 6146.
[100] G.W. Watson, R.P.K. Wells, D.J. Willock, G.J. Hutchings, Journal of Physical Chemistry B 105 (2001) 4889.
[101] N. Lopez, Z. Lodziana, F. Illas, M. Salmeron, Physical Review Letters 93 (2004).
[102] P. Ferrin, S. Kandoi, A.U. Nilekar, M. Mavrikakis, Surface Science 606 (2012) 679.
[103] J. Greeley, M. Mavrikakis, Journal of Physical Chemistry B 109 (2005) 3460.
[104] D.C. Ford, A.U. Nilekar, Y. Xu, M. Mavrikakis, Surface Science 604 (2010) 1565.
[105] L.J. Xu, Y. Xu, Catalysis Today 165 (2011) 96.
[106] M. Todorova, K. Reuter, M. Scheffler, Journal of Physical Chemistry B 108 (2004) 14477.
[107] J.F. Paul, P. Sautet, Physical Review B 53 (1996) 8015.
[108] D.O. Demchenko, G.M. Sacha, M. Salmeron, L.W. Wang, Surface Science 602 (2008) 2552.
[109] G. Novell-Leruth, A. Valcarcel, J. Perez-Ramirez, J.M. Ricart, Journal of Physical Chemistry C 111 (2007) 860.
[110] D.R. Alfonso, A.V. Cugini, D.S. Sholl, Surface Science 546 (2003) 12.
[111] S. Speller, T. Rauch, J. Bomermann, P. Borrmann, W. Heiland, Surface Science 441 (1999) 107.
[112] J. Bomermann, M. Huck, J. Kuntze, T. Rauch, S. Speller, W. Heiland, Surface Science 357 (1996) 849.
[113] M. Neurock, R.A. van Santen, Journal of Physical Chemistry B 104 (2000) 11127.
[114] J.F. Paul, P. Sautet, Journal of Physical Chemistry B 102 (1998) 1578.
[115] L. Gracia, M. Calatayud, J. Andres, C. Minot, M. Salmeron, Physical Review B 71 (2005).
[116] S.M. Kozlov, I.V. Yudanov, H.A. Aleksandrov, N. Rosch, Physical Chemistry Chemical Physics 11 (2009) 10955.
[117] G. Papapolymerou, V. Bontozoglou, Journal of Molecular Catalysis A—Chemical 120 (1997) 165.
[118] X. Guo, A. Hoffman, J.T. Yates, Journal of Physical Chemistry 93 (1989) 4253.
[119] J. Somers, M.E. Kordesch, T. Lindner, H. Conrad, A.M. Bradshaw, G.P. Williams, Surface Science 188 (1987) L693.
[120] J.J. Chen, N. Winograd, Surface Science 326 (1995) 285.
[121] M. Morkel, V.V. Kaichev, G. Rupprechter, H.J. Freund, I.P. Prosvirin, V.I. Bukhtiyarov, Journal of Physical Chemistry B 108 (2004) 12955.
[122] K. Jacobi, M. Bertolo, W. Hansen, Journal of Electron Spectroscopy and Related Phenomena 54 (1990) 529.
[123] M.E. Kordesch, T. Lindner, J. Somers, W. Stenzel, H. Conrad, A.M. Bradshaw, G.P. Williams, Spectrochimica Acta Part A—Molecular and Biomolecular Spectroscopy 43 (1987) 1561.
[124] M.E. Kordesch, W. Stenzel, H. Conrad, Journal of Electron Spectroscopy and Related Phenomena 39 (1986) 89.
[125] M.E. Kordesch, W. Stenzel, H. Conrad, Surface Science 175 (1986) L687.
[126] D. Loffreda, D. Simon, P. Sautet, Chemical Physics Letters 291 (1998) 15.
[127] D. Loffreda, D. Simon, P. Sautet, Journal of Chemical Physics 108 (1998) 6447.
[128] K.H. Hansen, Z. Sljivancanin, B. Hammer, E. Laegsgaard, F. Besenbacher, I. Stensgaard, Surface Science 496 (2002) 1.
[129] P.J. Chen, D.W. Goodman, Surface Science 297 (1993) L93.
[130] T.W. Kim, M.J. Weiss, C.J. Hagedorn, W.H. Weinberg, Journal of Vacuum Science & Technology A—Vacuum Surfaces and Films 19 (2001) 2941.
[131] B. Hammer, Y. Morikawa, J.K. Nøkrsov, Physical Review Letters 76 (1996) 2141.
[132] D. Loffreda, D. Simon, P. Sautet, Surface Science 425 (1999) 68.
[133] G. Rupprechter, M. Morkel, H.J. Freund, R. Hirschl, Surface Science 554 (2004) 43.
[134] M. Rebholz, N. Kruse, Journal of Chemical Physics 95 (1991) 7745.
[135] D. Stacchiola, Y. Wang, W.T. Tysoe, Surface Science 524 (2003) 173.
[136] F. Solymosi, J. Rasko, Journal of Catalysis 155 (1995) 74.
[137] A.A. Phatak, W.N. Delgass, F.H. Ribeiro, W.F. Schneider, Journal of Physical Chemistry C 113 (2009) 7269.
[138] Y.L. Cao, Z.X. Chen, Surface Science 600 (2006) 4572.